Bull. Mater. Sci. (2019) 42:102
https://doi.org/10.1007/s12034-019-1804-6

Role of synthesis of upconversion nanoparticles towards surface modification and photocatalysis

SWAPNA CHALLAGULLA, SOUMITRA PAYRA, MAYUR BAJAJ and SOUNAK ROY*
Department of Chemistry, Birla Institute of Technology and Science (BITS) Pilani, Hyderabad Campus, Jawahar Nagar, Shameerpet Mandal, Hyderabad 500078, India
*Author for correspondence (sounak.roy@hyderabad.bits-pilani.ac.in)

MS received 23 August 2018; accepted 15 November 2018; published online 27 March 2019

Abstract. TiO_2 being a wide band gap semiconducting material cannot use the solar insolation for photocatalysis. An interesting strategy is to dope TiO_2 with upconverting rare earth materials, which upon infrared (IR) or visible light irradiation can emit ultraviolet light to generate excitons in TiO_2 for further catalytic reactions. This manuscript reports the incorporation of Er_2O_3/Yb_2O_3 into TiO_2 *via* two synthetic methodologies. One of which yields the co-presence of rare earth oxides and TiO_2 on the surface, while the other synthetic route yields the rare earth oxides in the core of the TiO_2 shell. The detailed structural, morphological and optical properties of the laboratory synthesized materials were studied by powder XRD, FE-SEM, STEM, HR-TEM, BET, UV-DRS and PL. The surfaces of the materials did show some difference in their properties depending on their synthesis route, however, the two photon excitation was similar to both the set of materials. The synthesized materials were studied for degradation of rhodamine B dye, and the results suggested that the presence of Er_2O_3/Yb_2O_3 on the TiO_2 surface was detrimental for catalytic application, while TiO_2 exposed on the surface with Er_2O_3/Yb_2O_3 in the core can be a choice of materials for photocatalytic application.

Keywords. Photocatalysis; upconversion; rare earth metal oxide; TiO_2; rhodamine B.

1. Introduction

TiO_2 is one of the most widely investigated semiconductor catalytic materials for a broad range of photocatalytic applications. However, the primary problem associated with TiO_2 is the high band gap (~3.3), which makes the material incompatible under solar insolation. UV light can produce excitons in TiO_2, however, there is only 3–5% of UV radiation in sun light. Plethora of investigation has involved in engineering the band gap of TiO_2 mostly by doping of anions and cations [1–7], involving dyes [8,9], surface modification [10,11] and coupling with other semiconductors [12,13] for absorbing the photonic energy from the visible solar spectrum. In spite of this effort, there is room for significant improvements towards better capturing of solar light, and consequent catalytic efficiency. Instead of these existing ideas of tailoring of the band gap, an interesting approach is to transform the low energy solar light into high energy ultraviolet photons by incorporating upconverting rare earth element into TiO_2. The upconverting rare earth materials, due to the presence of f and d orbitals, when pumped by infrared (IR) or visible light sources, emit light of ultraviolet photon energy *via* an anti-Stokes process [14–16]. This secondary ultraviolet light source can generate excitons in TiO_2 for further catalytic reactions. It has also been proposed that doping with rare earth metals not only helps in upconversion, but also reduces the electron–hole recombination rates *via* charge trapping [17,18]. Er^{3+} and Yb^{3+} among all the f-block ions have gained considerable attention for energy upconverting metals [19–24].

Recently, this approach is getting popularize as evident by the increasing number of studies [25–29]. Pickering *et al* have studied Yb^{3+}/Er^{3+}/Y-Al garnet/TiO_2 for rose bengal dye degradation, and observed upconversion and lesser electron–hole recombination over this composite [30]. Singh *et al* [31] have incorporated Er^{3+} on the mesoporous spheres of TiO_2, and the photocatalytic efficiency was found to be better than that of pristine TiO_2. The β-$NaYF_4$:Yb^{3+}, Tm^{3+}@TiO_2 core@shell material has shown promising photochemical and photoelectrical applications [32]. Er and Yb were also doped in the anatase lattice of TiO_2 for phenol degradation under simulated solar irradiation [33]. Apparently, in literature there are evidences of rare earth oxides being incorporated in the surface and in the core of TiO_2. Depending on the structure, the photocatalytic efficacy also varied. TiO_2 has a unique surface for catalytic reactions. The surface –OH groups on interaction with the photo-excited holes may produce the key species of surface $HO^{\bullet}$ radicals for degradation reactions. The presence of the rare earth oxides may play a detrimental role in catalytic efficacy. However, the upconverting rare-earth oxides are essential for near-infrared (NIR) or visible light utilization. Therefore, in this work,

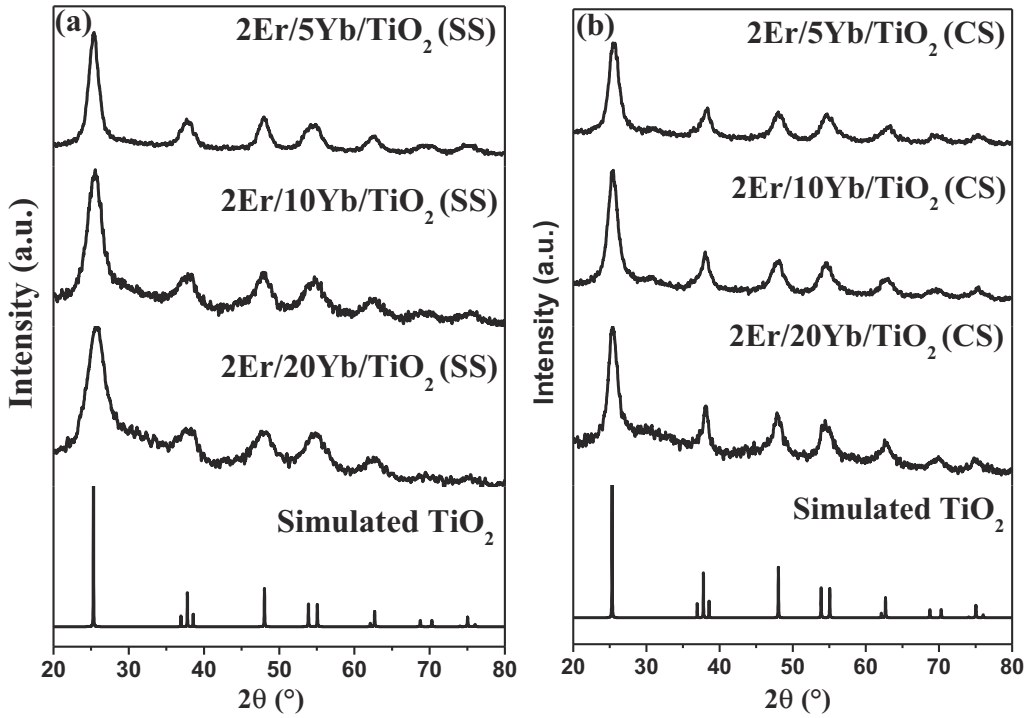

Figure 1. XRD patterns of (**a**) Er/Yb/TiO_2 (SS) and (**b**) Er/Yb/TiO_2 (CS).

Table 1. Crystallite size, SSA, pore volume, average pore size, and the band gap of both Er/Yb/TiO_2 (SS) and Er/Yb/TiO_2 (CS).

Material	Crystallite size (nm)	SSA ($m^2\ g^{-1}$)	Pore volume ($cm^3\ g^{-1}$)	Pore size (nm)	Band gap (E_g) (eV)
2Er/5Yb/TiO_2 (SS)	5.27	179.57	0.26	5.87	3.79
2Er/10Yb/TiO_2 (SS)	3.64	235.37	0.25	4.27	3.84
2Er/20Yb/TiO_2 (SS)	2.58	236.79	0.18	3.10	3.8
2Er/5Yb/TiO_2 (CS)	5.16	248.35	0.35	5.66	3.6
2Er/10Yb/TiO_2 (CS)	5.19	250.20	0.35	5.67	3.78
2Er/20Yb/TiO_2 (CS)	6.13	272.02	0.34	5.05	3.85

we have addressed the issue of incorporation of rare earth oxides in the surface and core of TiO_2 to evaluate its catalytic efficacy.

Here, Er_2O_3 was selected as the primary rare earth oxide, as it has comparatively high upconversion efficacy among the other rare earth oxides, and the concentration was kept constant at 2 at% [30,34–37]. Yb_2O_3 was chosen as the sensitizer in combination with Er_2O_3, and the concentration was varied from 5, 10 and 20 at%. The $Er_2O_3/Yb_2O_3/TiO_2$ composite was synthesized by two different synthetic routes in order to place the rare earth oxides along with the TiO_2 surface, and also as the core of the TiO_2 shell. The materials were thoroughly characterized and their photocatalytic efficacy to degrade the dye rhodamine B was investigated. The role of rare earth oxides in the surface and in the core towards catalytic efficacy was evaluated.

2. Experimental

Titanium(IV) isopropoxide ($Ti[OCH(CH_3)_2]_4$), erbium nitrate ($Er(NO_3)_3{\cdot}5H_2O$) and ytterbium nitrate ($Yb(NO_3)_3{\cdot}5H_2O$) were purchased from Sigma-Aldrich. Glycine (NH_2CH_2COOH) and isopropyl alcohol ($(CH_3)_2CHOH$) were procured from SD-Fine chemicals.

2.1 *One step synthesis*

In the single step synthesis, the supported oxide was synthesized by a solution combustion method. Initially, titanium isopropoxide was completely hydrolysed with water, and was dissolved in concentrated HNO_3 to synthesize the titanyl nitrate precursor. Then the required amounts of aqueous solution of erbium nitrate, ytterbium nitrate and titanyl nitrate

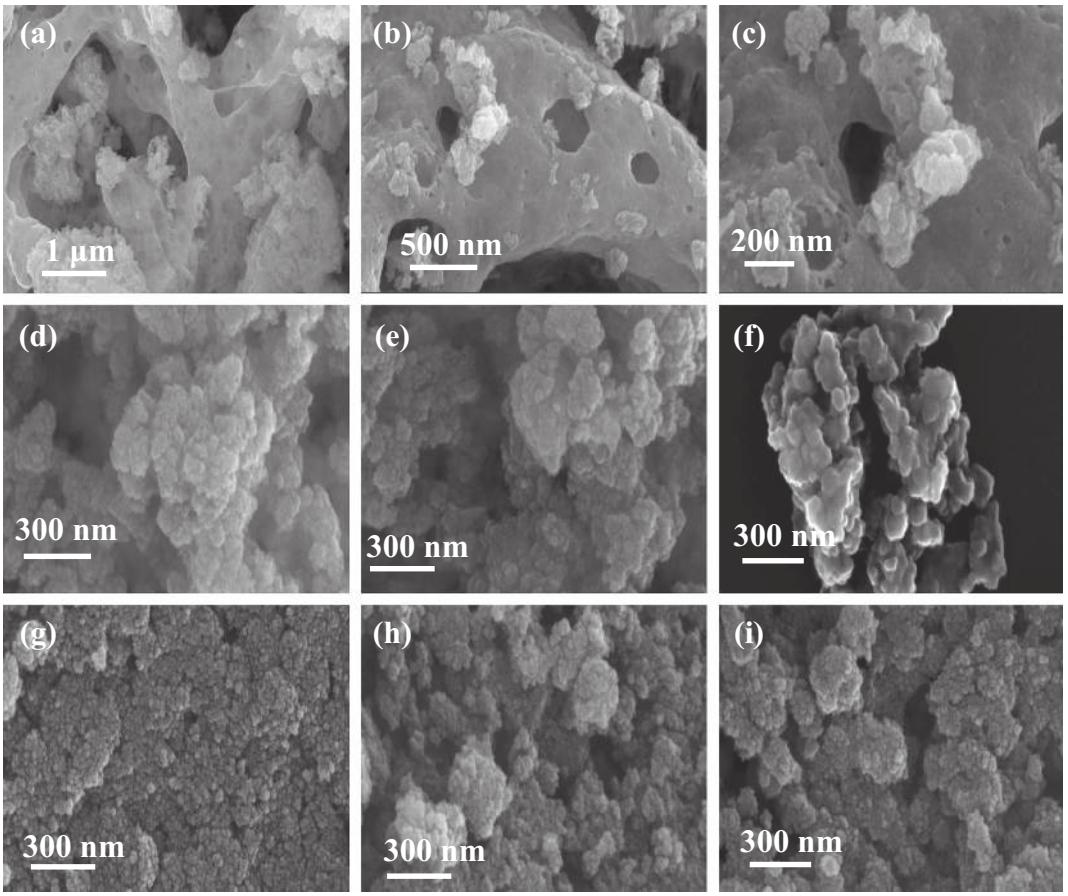

Figure 2. The FE-SEM images of (**a–c**) Er_2O_3/Yb_2O_3, (**d**) 2Er/5Yb/TiO_2 (SS), (**e**) 2Er/10Yb/TiO_2 (SS), (**f**) 2Er/20Yb/TiO_2 (SS), (**g**) 2Er/5Yb/TiO_2 (CS), (**h**) 2Er/10Yb/TiO_2 (CS) and (**i**) 2Er/20Yb/TiO_2 (CS).

prepared from titanium isopropoxide were mixed in a borosilicate dish. Glycine was added to it as fuel for combustion, and the reaction mixture was placed in a muffle furnace which was pre-heated at 450°C. The solution was heated, and Er/Yb/TiO_2 was obtained. The Er concentration was kept constant at 2 at%, while Yb concentration was varied from 5, 10 and 20 at%. This single step synthesized materials will be designated in the manuscript as 2Er/NYb/TiO_2 (SS), where $N = 5$, 10 and 20.

2.2 *Two step synthesis*

The double step synthesis was carried out in order to procure core–shell type materials. In the first step Er_2O_3/Yb_2O_3 was synthesized by solution combustion synthesis as mentioned earlier. The as-prepared rare earth oxides along with titanium(IV) isopropoxide were suspended in isopropyl alcohol with vigorous stirring. Water was added dropwise to this suspension while stirring. After one hour of continuous stirring, the product was filtered off, and was heated at 120°C for 4 h to procure the core–shell 2Er/NYb/TiO_2 (CS) (where $N = 5$, 10 and 20).

2.3 *Characterization*

The structural information was obtained from powder X-ray diffraction (PXRD) analyses of the as-synthesized materials and analyses were carried out with Rigaku Ultima IV. The surface morphology of the catalysts was measured by field emission scanning electron microscopy (FE-SEM) and scanning transmission electron microscopy (STEM) using FEI-Apreo S apparatus. The high resolution transmission electron microscopy (HR-TEM) images of the catalysts were collected with a JEOL 2010 EX microscope. The surface area and porosity of the synthesized materials was determined using a Microtrac BEL Corp mini-II surface area analyser by using a nitrogen adsorption/desorption method. Diffuse reflectance spectra (DRS) were recorded by solid state UV measurements on a JASCO V-670 to study the upconversion, and the band gaps of 2Er/NYb/TiO_2 (SS) and 2Er/NYb/TiO_2 (CS) materials. The Kubelka–Munk function $(1 - R)^2/2R$ *vs.* E (where E is the energy of light and R is the reflectance) was plotted from reflectance spectra in order to calculate the bandgaps. The upconversion luminescence (UCL) spectra were recorded using a JASCO FP-6300 spectrophotometer with an excitation wavelength of 290 nm. UCL spectra were

also collected with an excitation wavelength of 980 nm using an Agilent Technologies Cary Eclipse fluorescence spectrophotometer.

2.4 *Photocatalysis*

The photocatalytic degradation of rhodamine B was studied with a visible lamp of 250 W (HPS 250), to mimic the solar light. For each experiment, about 100 ml of 5 ppm of rhodamine B solution was taken with a catalyst loading of 50 mg. To attain an adsorption equilibrium of rhodamine B over the catalyst surfaces, initially the solution was stirred in the dark for 30 min following which, visible light was used to irradiate the reaction mixture under aerobic conditions. Periodically, 2 ml of aliquot was withdrawn, centrifuged in order to remove the catalyst, and the absorbance was measured by using a JASCO V-650 to find out the concentration of rhodamine B with progress of the reaction.

The concentration of the key reaction species and surface $HO^{\bullet}$ were measured by converting coumarin to umbelliferone. About 15 mg of Er/Yb/TiO_2 (SS) and Er/Yb/TiO_2 (CS) samples were dispersed in 3.5 ml of aqueous solution of coumarin (0.1 mM) in a quartz cuvette, and were exposed to visible light irradiation for 150 min. Following which, 0.5 g of KCl was added into the irradiated suspension, and then the suspension was kept in the dark for 12 h. After sedimentation of the catalyst, fluorescence of the clear solution was measured by using an excitation wavelength of umbelliferone at 332 nm.

3. Results and discussion

The PXRD profiles of the synthesized catalysts are shown in figure 1. All the six materials crystallized in the pure anatase phase. None of the catalysts showed any signature peak of Yb_2O_3 or Er_2O_3 concluding the rare earth oxides being in a well-dispersed state or amorphous state. It is evident from figure 1a and b that with increased Yb_2O_3 oxide concentration the crystallinity of TiO_2 was significantly decreased with the single step synthesized supported oxides, and the same was not that significant over core–shell materials. This could be due to the more surface exposure of amorphous rare earth oxides in 2Er/20Yb/TiO_2 (SS) than that in 2Er/20Yb/TiO_2 (CS). The crystallite size of the materials was calculated by Scherrer's equation from the anatase (101) peak broadening and the obtained values are presented in table 1. The overall crystallite sizes of Er/Yb/TiO_2 (CS) were found to be higher than that of Er/Yb/TiO_2 (SS) concluding more nanostructures of the core–shell material. With increasing concentration of Yb_2O_3, the crystallite sizes of Er/Yb/TiO_2 (CS) remained unchanged, however, for Er/Yb/TiO_2 (SS) the crystallite sizes gradually decreased.

Figure 2 represents the FE-SEM images of the Er/Yb/TiO_2 (CS) and Er/Yb/TiO_2 (SS) materials of different magnifications. Er_2O_3/Yb_2O_3 prepared by the solution combustion method without TiO_2 support showed a wide distribution size of particles with high porosity as shown in figure 2a–c. In the Er/Yb/TiO_2 (SS) and Er/Yb/TiO_2 (CS) materials the porosity was not observed, and also the particle sizes were more uniform and smaller (figure 2d–i). With higher concentration of Yb_2O_3, the particles became more fused and larger in size in Er/Yb/TiO_2 (SS). However, there was no significant difference in the morphology of Er/Yb/TiO_2 (CS) with increasing concentration of Yb_2O_3.

To confirm the formation of the core–shell structure of Er/Yb/TiO_2 (CS), we have performed the STEM imaging for Er/Yb/TiO_2 (CS) samples (figure 3). The STEM images show the formation of a core–shell for 2Er/5Yb/TiO_2 (CS), and also the rare earth core is very small. The images of

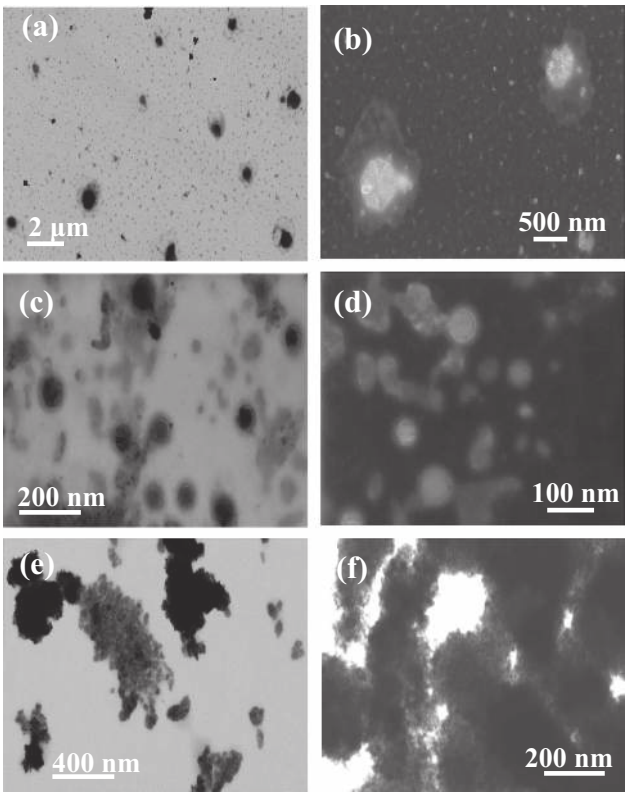

Figure 3. The STEM images of (**a, b**) 2Er/5Yb/TiO_2 (CS), (**c, d**) 2Er/10Yb/TiO_2 (CS) and (**e, f**) 2Er/20Yb/TiO_2 (CS).

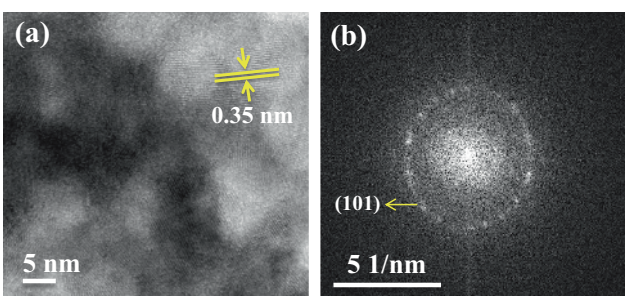

Figure 4. (**a**) HR-TEM image and (**b**) its selected area electron diffraction pattern of 2Er/10Yb/TiO_2 (CS).

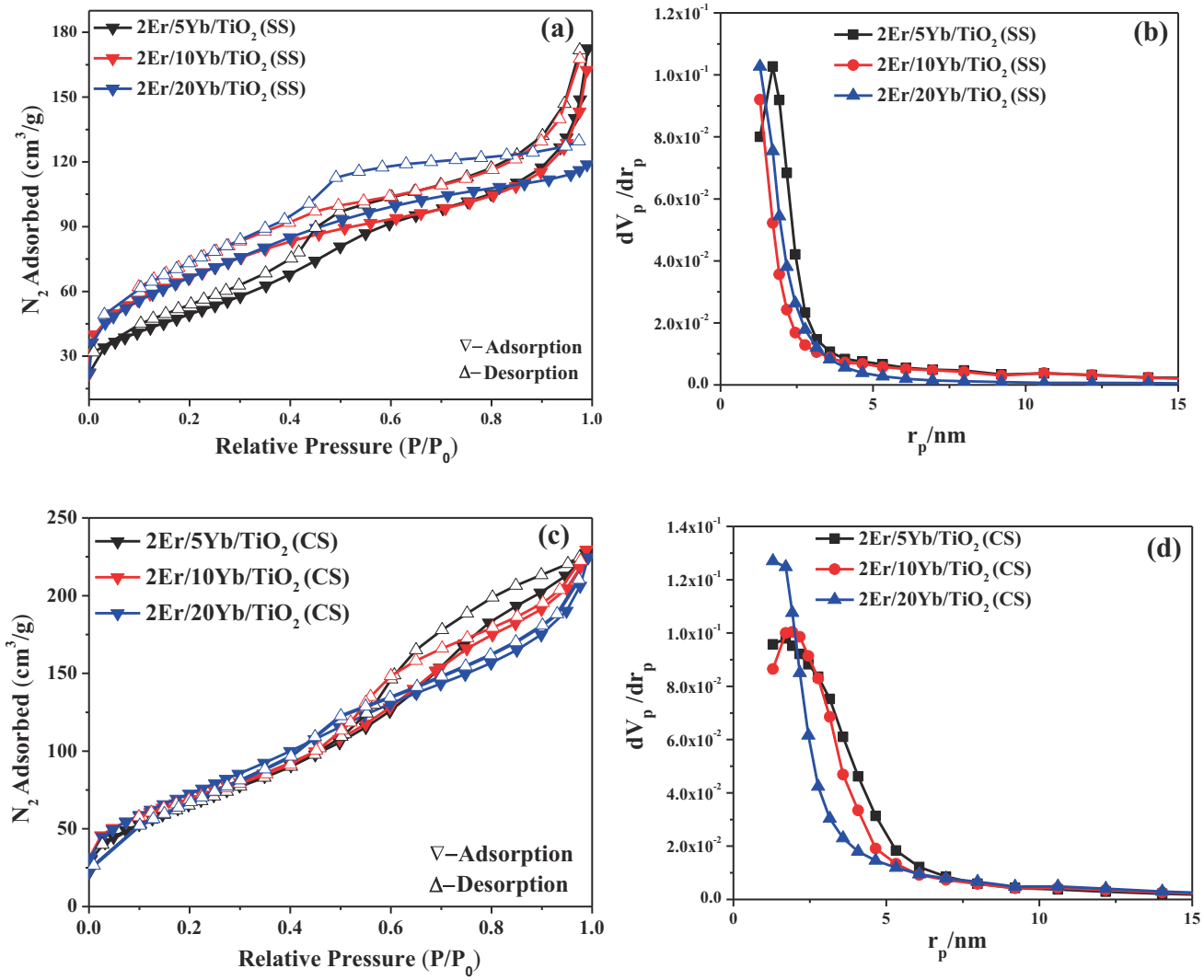

Figure 5. N_2 adsorption–desorption isotherms and pore size distribution of (**a, b**) Er/Yb/TiO_2 (SS) and (**c, d**) Er/Yb/TiO_2 (CS).

2Er/10Yb/TiO_2 (CS) also confirm the core–shell structure, however, compared with 2Er/5Yb/TiO_2 (CS) the core size of 2Er/10Yb/TiO_2 (CS) is bigger. It must be noted from the images that not all the particles are coated uniformly. With a further increase in the amount of Yb_2O_3, there was no core–shell type structure for 2Er/20Yb/TiO_2 (CS). This indicates that there is an optimum ratio of rare-earth to TiO_2 in order to form the core–shell structure. With a higher amount of Yb_2O_3, a lower concentration of TiO_2 may not be sufficient enough to encapsulate the rare-earth oxide to form a shell.

The representative HR-TEM images of 2Er/10Yb/TiO_2 (CS) in figure 4 corroborate the findings from FE-SEM and STEM studies. The high resolution image shows a fringe distance of 0.35 nm, corresponding to the (101) plane of anatase TiO_2 and the selected area electron diffraction pattern also shows the (101) plane of anatase TiO_2. There were no lattice fringes corresponding to Yb_2O_3 or Er_2O_3 as in FE-SEM and STEM studies.

The BET specific surface area (SSA), pore volume, and mean pore sizes of the synthesized materials were derived from adsorption isotherms as shown in figure 5, and presented in table 1. Evidently, the BET surface areas of the Er/Yb/TiO_2 (CS) were higher than those of Er/Yb/TiO_2 (SS) for any given concentration of Yb_2O_3. The occurrence of rare earth oxides on the surfaces of TiO_2 in Er/Yb/TiO_2 (SS) samples might have reduced the (SSA). In contrast, in Er/Yb/TiO_2 (CS) samples, as mostly the rare earth materials stayed in the core, the TiO_2 surface area was not affected. It was interesting to find out that with higher concentration of Yb_2O_3, the surface area was steadily increased. The impact of rare earth oxides being present in the surface or core was also evident with mean pore sizes. With the increasing amount of rare earth oxides in the core, mean pore sizes remain unaffected for Er/Yb/TiO_2 (CS) materials, whereas, the increasing concentration of rare earth oxides on the surface has reduced the pore sizes of Er/Yb/TiO_2 (CS) materials. As catalysis is a surface

phenomenon, this may impact on the catalytic efficacy of the materials.

The DRS spectra (figure 6a) showed that the incorporation of rare earth oxides produces absorption bands in the visible and NIR regions. No such upconversion peak was observed over the pristine TiO_2 sample. The DRS profiles of Er/Yb/TiO_2 (SS) samples were more similar to pristine TiO_2, while Er/Yb/TiO_2 (CS) samples showed sharp rise after point of inflection at 315 nm. In addition, in NIR, the rare earth oxide doped TiO_2 had a prominent peak at 980 nm corresponding to the $4I_{11/2}$ transition. This peak intensity is increased with higher concentration of Yb_2O_3. This could be due to the enhanced IR absorption because of a combination of Yb and Er rare earth metals [33]. The combination of these wide visible and NIR absorption features renders the possibility of a broad photo-response. The Tauc plots were built from DRS spectra to obtain the band gap (figure 6b), and results are given in table 1. The obtained values are all within the general band gap range of anatase TiO_2 to be ~3 eV. A slight increase in the band gap had been observed with higher Yb_2O_3 concentration, which indicates partial doping of rare earth metals within the TiO_2 lattice. The PL spectra of the synthesized catalysts excited at 290 nm are shown in figure 7a. Er/Yb/TiO_2 (CS) showed a broad band at 400 nm, which was not observed for Er/Yb/TiO_2 (SS). This broad band could be due to the anatase lattice distortions induced by defects [33]. Both the set of materials showed a sharp peak at 470 nm. The intensity of this peak was higher in Er/Yb/TiO_2 (CS) compared to Er/Yb/TiO_2 (SS). To check the upconversion ability of these catalysts, the PL spectra were also collected after excitation at 980 nm, and are shown in figure 7b and c. The major visible range peaks were observed at 487 and 700 nm, and a broad high intense peak at 800 nm. The visible light peak intensities of the core–shell materials were found to be higher than those of the materials synthesized by single step.

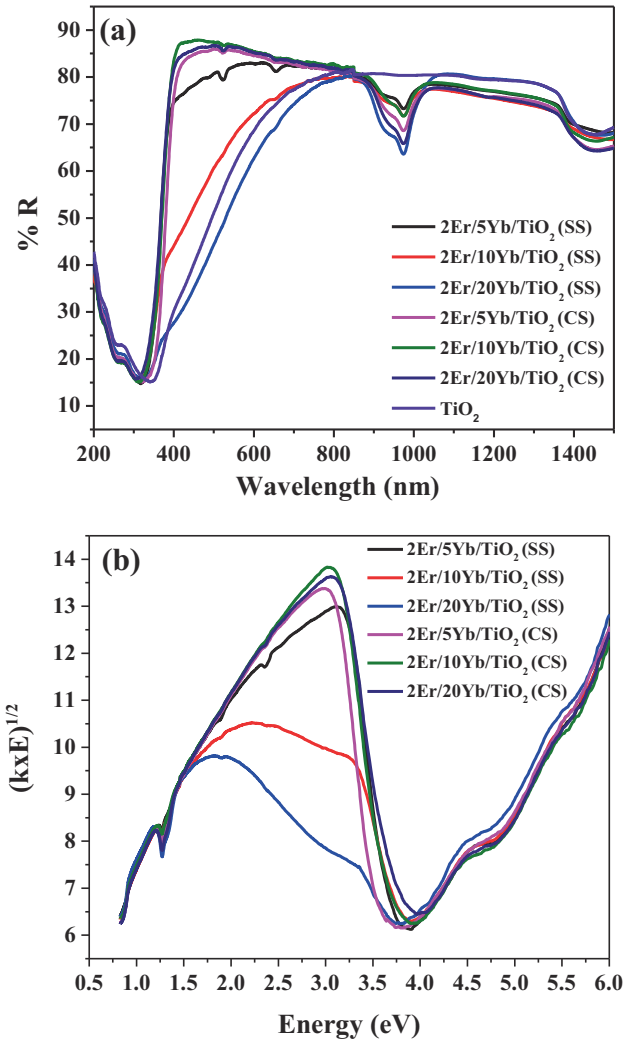

Figure 6. (**a**) Diffuse reflectance UV–vis spectra and (**b**) Tauc plot of the synthesized catalysts.

As the materials showed a promising upconversion of the NIR to visible range, the photocatalytic activity of Er/Yb/TiO_2 (SS) and Er/Yb/TiO_2 (CS) materials was assessed by the photodegradation of rhodamine B under visible light irradiation (figure 8). A graph of C/C_0 *vs.* time was ploted in figure 8, where C_0 and C are the concentrations of rhodamine B at time $t = 0$, and at time t, respectively. It is evident from the figure that both 2Er/5Yb/TiO_2 (SS) and 2Er/5Yb/TiO_2 (CS) completely degrade rhodamine B under simulated light irradiation in 3 h, and the reaction efficacies are also comparable. The initial rate of degradation was obtained to be 9×10^{-3} and 9.5×10^{-3} mol l^{-1} min^{-1} for 2Er/5Yb/TiO_2 (SS) and 2Er/5Yb/TiO_2 (CS) materials, respectively. However, with an increase in Yb_2O_3 concentration, there was no significant alteration in the reaction efficacy of Er/Yb/TiO_2 (CS), but, the rate of reaction over Er/Yb/TiO_2 (SS) decreased gradually. The gradual decrease in reactivity can be explained by the surface properties (*vide* FE-SEM, STEM and SSA discussion). Upon light irradiation, the NIR part of the visible light absorbed by the upconversion particles of Er_2O_3/Yb_2O_3 is converted into high energy light. This high energy light on semiconducting TiO_2 excites the electrons to the conduction band leaving a positive hole in the valance band (equation 1). The catalytic unique surface of TiO_2 possesses the surface hydroxyl groups, which on reaction with holes can produce reactive $HO^{\bullet}$ (equation 2). The photodegradation of rhodamine B is primarily mediated by this highly reactive surface oxygen species of $HO^{\bullet}$ (equation 3) [38,39].

$$\text{Er/Yb/TiO}_2 \xrightarrow{h\nu} e^-_{CB} + h^+_{VB} \quad (1)$$

$$h^+_{VB} + \text{Ti-OH} \rightarrow HO^{\bullet} \quad (2)$$

$$C_{28}H_{31}ClN_2O_3 + HO^{\bullet} \rightarrow 28CO_2 + 14H_2O + HCl + 2HNO_3 \quad (3)$$

In the single step solution combustion, synthesized Er/Yb/TiO_2 (SS) materials possess Er_2O_3/Yb_2O_3 oxides on the surface of TiO_2. With a higher amount of Yb_2O_3, there is less

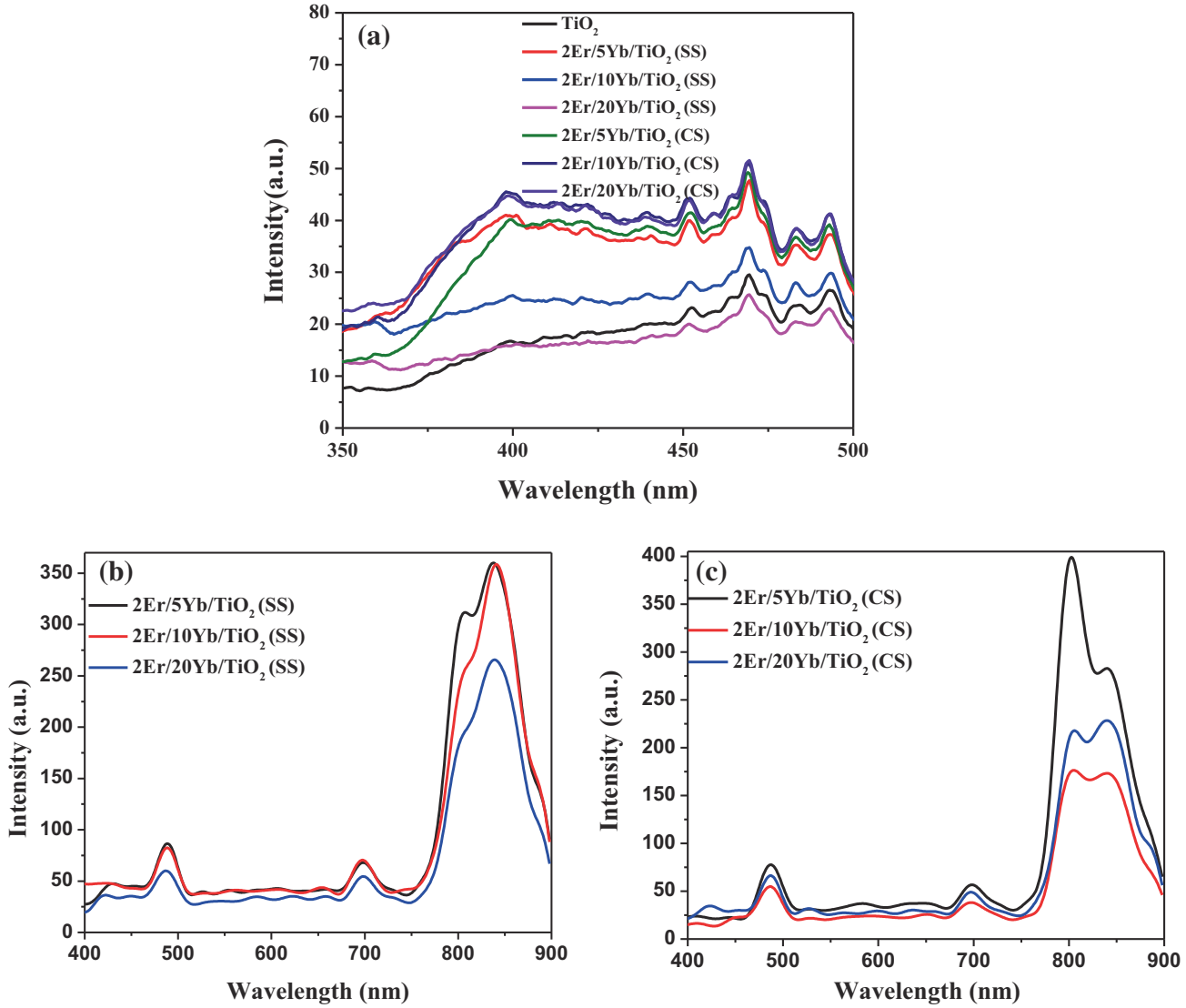

Figure 7. PL spectra of the synthesized catalysts at (**a**) 290 nm excitation and (**b, c**) 980 nm excitation.

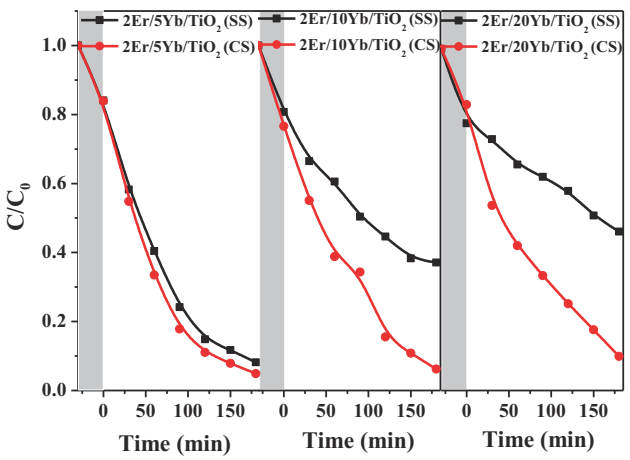

Figure 8. Photodegradation of rhodamine B under visible light irradiation.

exposure of surface TiO_2 in Er/Yb/TiO_2 (SS), as found from STEM images, and this may produce less reactive OH•, which can decrease in the rate of rhodamine B degradation. In contrast, in the core–shell 2Er/5Yb/TiO_2 (CS) the surface is mostly dominated by TiO_2, and therefore, the rate of photodegradation was not affected (scheme 1).

To verify it further, we have probed the OH• generated from surface TiO_2 over Er/Yb/TiO_2 (SS) and Er/Yb/TiO_2 (CS) under visible light irradiation. For the detection of OH• coumarin was used as a fluorescent probe. The surface OH• reacts with coumarin to generate a strong fluorescent emitter, 7-OH coumarin (umbelliferone). Figure 9 represents the concentration of umbelliferone with time over 2Er/10Yb/TiO_2 (SS) and 2Er/10Yb/TiO_2 (CS) under visible light irradiation. Interestingly, production of OH• was minimal over 2Er/10Yb/TiO_2 (SS), whereas 2Er/10Yb/TiO_2 (CS) showed significant OH• production. This was in accordance with

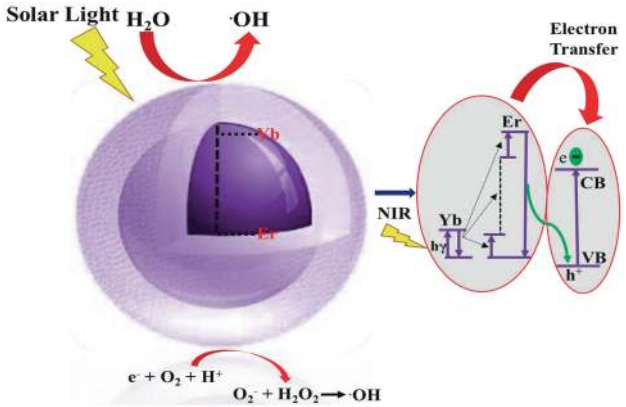

Scheme 1. Schematic representation of the reaction mechanism.

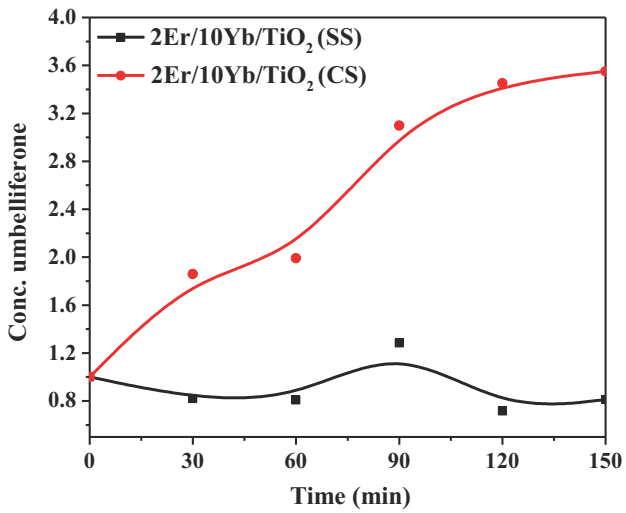

Figure 9. Concentration of umbelliferone *vs.* visible light irradiation time over 2Er/10Yb/TiO_2 (SS) and 2Er/10Yb/TiO_2 (CS).

the proposed reaction mechanism and the photodegradation results. The more exposed TiO_2 on the surface with Er_2O_3/Yb_2O_3 in the core can be a choice of materials for photocatalytic application.

4. Conclusion

Er/Yb/TiO_2 with varied concentrations of Yb was synthesized by two methods, namely single step solution route and dual step core–shell route. Er/Yb/TiO_2 (CS) possessed a higher surface area and porosity compared to its homologue prepared by the combustion route. Presence of TiO_2 on the surface of Er/Yb/TiO_2 (CS) and not on Er/Yb/TiO_2 (SS) resulted in the production of more surface $OH^\bullet$ species. Upon irradiation of solar light, the upconversion material Er_2O_3/Yb_2O_3 converted the low energy light to high energy light, which produced h^+_{VB} in the TiO_2 shell, and consequently reactive surface $OH^\bullet$ for further photodegradation of dye.

Acknowledgements

SR thanks Department of Science and Technology—fund for improvement of science and technology infrastructure (DST FIST; SR/FST/CSI-240/2012). The authors thank BITS Pilani, Hyderabad campus for providing research facilities. We also thank Dr Venkata Krishnan and his group at IIT Mandi for the upconversion luminescence measurements.

References

[1] Li D, Ohashi N, Hishita S, Kolodiazhnyi T and Haneda H 2005 *J. Solid State Chem.* **178** 3293
[2] Barolo G, Livraghi S, Chiesa M, Paganini M C and Giamello E 2012 *J. Phys. Chem. C* **116** 20887
[3] Wang J, Sun H, Huang J, Li Q and Yang J 2014 *J. Phys. Chem. C* **118** 7451
[4] Livraghi S, Chierotti M R, Giamello E, Magnacca G, Paganini M C, Cappelletti G *et al* 2008 *J. Phys. Chem. C* **112** 17244
[5] Long R and English N J 2011 *Phys. Rev. B* **83** 155209
[6] Liu Y, Zhou W, Liang Y, Cui W and Wu P 2015 *J. Phys. Chem. C* **119** 11557
[7] Liu Q, Ding D, Ning C and Wang X 2015 *Int. J. Hydrog. Energy* **40** 2107
[8] Cho Y, Choi W, Lee C H, Hyeon T and Lee H I 2001 *Environ. Sci. Technol.* **35** 966
[9] Wang Q, Chen C, Zhao D, Ma W and Zhao J 2008 *Langmuir* **24** 7338
[10] Ren J, Wang W, Sun S, Zhang L and Chang J 2009 *Appl. Catal. B Environ.* **92** 50
[11] Zhu S, Xu T, Fu H, Zhao J and Zhu Y 2007 *Environ. Sci. Technol.* **41** 6234
[12] Kamat P V 1993 *Chem. Rev.* **93** 267
[13] Kumar S G and Devi L G 2011 *J. Phys. Chem. A* **115** 13211
[14] Kar A, Kundu S and Patra A 2015 *ChemPhysChem* **16** 505
[15] Auzel F 2004 *Chem. Rev.* **104** 139
[16] Wang F and Liu X 2009 *Chem. Soc. Rev.* **38** 976
[17] Obregón S, Kubacka A, Fernández-García M and Colón G 2013 *J. Catal.* **299** 298
[18] Reszczyńska J, Grzyb T, Sobczak J W, Lisowski W, Gazda M, Ohtani B *et al* 2015 *Appl. Catal. B Environ.* **163** 40
[19] Salhi R and Deschanvres J L 2016 *J. Luminescence* **176** 250
[20] Wang M, Mi C C, Wang W X, Liu C H, Wu Y F, Xu Z R *et al* 2009 *ACS Nano* **3** 1580
[21] Bai X, Song H, Pan G, Lei Y, Wang T, Ren X *et al* 2007 *J. Phys. Chem. C* **111** 13611
[22] Li Y, Zhang J, Zhang X, Luo Y, Ren X, Zhao H *et al* 2009 *J. Phys. Chem. C* **113** 4413
[23] Kar A and Patra A 2012 *Nanoscale* **4** 3608
[24] Patra A, Friend C S, Kapoor R and Prasad P N 2003 *Chem. Mater.* **15** 3650
[25] Bian W, Wang T, Guo Y, Yu X, Xu X and Qiu J 2015 *Cryst. Eng. Comm.* **17** 7332

[26] Singh V, Kumar Rai V and Haase M 2012 *J. Appl. Phys.* **112** 063105
[27] Wang X, Zhang Z, Qin J, Shi W, Liu Y, Gao H *et al* 2017 *Electrochimica Acta* **245** 839
[28] Rojas-Hernandez R E, Barradas N P, Alves E, Santos L F and Almeida R M 2018 *Surf. Coat. Technol.* **355** 162
[29] Balaji R, Kumar S, Reddy K L, Sharma V, Bhattacharyya K and Krishnan V 2017 *J. Alloys Compd.* **724** 481
[30] Pickering J W, Bhethanabotla V R and Kuhn J N 2017 *Appl. Catal. B Environ.* **202** 147
[31] Singh K, Harish S, Kristy A P, Shivani V, Archana J, Navaneethan M *et al* 2018 *Appl. Surf. Sci.* **449** 755
[32] Xu D X, Lian Z W, Fu M L, Yuan B, Shi J W and Cui H J 2013 *Appl. Catal. B Environ.* **142** 77
[33] Bhethanabotla V C, Russell D R and Kuhn J N 2017 *Appl. Catal. B Environ.* **202** 156
[34] Zhang J, Huang Y, Jin L, Rosei F, Vetrone F and Claverie J P 2017 *ACS Appl. Mater. Interfaces* **9** 8142
[35] De G, Qin W, Zhang J, Zhang J, Wang Y, Cao C *et al* 2006 *J. Luminescence* **119** 258
[36] Gonell F, Haro M, Sánchez R S, Negro P, Mora-Seró I, Bisquert J *et al* 2014 *J. Phys. Chem. C* **118** 11279
[37] Tamilmani V, Soni A K, Rai V K, Nair B U and Sreeram K J 2017 *J. Chem. Sci.* **129** 1929
[38] Yu K, Yang S, He H, Sun C, Gu C and Ju Y 2009 *J. Phys. Chem. A* **113** 10024
[39] He Z, Yang S, Ju Y and Sun C 2009 *J. Environ. Sci.* **21** 268